PROTEINS: Structure, Function, and Genetics 16:155–171 (1993)

Structure Determination of Feline Panleukopenia Virus Empty Particles

Mavis Agbandje,[1] Robert McKenna,[1] Michael G. Rossmann,[1] M. Lisa Strassheim,[2] and Colin R. Parrish[2]

[1]Department of Biological Sciences, Purdue University, West Lafayette, Indiana 47907, and [2]James A. Baker Institute for Animal Health, New York State College of Veterinary Medicine, Cornell University, Ithaca, New York 14853

ABSTRACT **Various crystal forms of the single-stranded DNA, feline panleukopenia virus (FPV), a parvovirus, have been grown of both full virions and empty particles. The structure of empty particles crystallized in an orthorhombic space group $P2_12_12_1$, with unit cell dimensions a = 380.1 Å, b = 379.3 Å, and c = 350.9 Å, has been determined to 3.3 Å resolution. The data were collected using oscillation photography with synchrotron radiation. The orientations of the empty capsids in the unit cell were determined using a self-rotation function and their positions were obtained with an *R*-factor search using canine parvovirus (CPV) as a model. Phases were then calculated, based on the CPV model, to 6.0 Å resolution and gradually extended to 3.3 Å resolution by molecular replacement electron density averaging. The resultant electron density was readily interpreted in terms of the known amino acid sequence. The structure is contrasted to that of CPV in terms of host range, neutralization by antibodies, hemagglutination properties, and binding of genomic DNA.** © 1993 Wiley-Liss, Inc.

Key words: parvovirus, feline, structure, comparison with canine virus, host range, antigenicity, hemagglutination

INTRODUCTION

Feline panleukopenia virus (FPV) is a member of the feline parvovirus subgroup of the autonomous parvovirus genus of the Parvoviridae family.[1] Parvoviruses are small spherical, nonenveloped icosahedral viruses with a diameter of about 260 Å, containing a linear single-stranded DNA genome of approximately 5,000 bases. Parvoviruses have a wide range of hosts, including humans, cats, dogs and mink. FPV infects cats, which can result in fatality, especially in kittens, due to the tendency of the autonomous parvoviruses to be very destructive to highly proliferating cells such as those of the cerebellum, lymphoid tissue and intestinal epithelium (reviewed in Parrish[2]). Both full (DNA containing) and empty particles are formed in tissue culture, have a sedimentation coefficient of 110 S and 70 S and band in isopycnic CsCl gradients at densities of 1.41 and 1.32 g/cm^3, respectively. The molecular weight of the full virion is 5.5–6.2 × 10^6 Da, of which 1.6 × 10^6 Da is DNA. The molecular weight of the empty particles is 4.2 × 10^6 Da. The mature FPV virion contains three capsid proteins, VP-1, VP-2, and VP-3, with molecular weights of 83, 67, and 65 kDa, respectively. The VP-1 and VP-2 proteins are formed from alternative start codons as a consequence of differential splicing of the messenger RNA from the viral DNA.[3] Thus the entire amino acid sequence of VP-2 is contained within VP-1. In full infectious virions, but not in empty particles, VP-3 is derived from VP-2 by proteolytic cleavage of 15 to 18 amino acid residues from the amino terminus.

FPV is closely related to canine parvovirus (CPV; Table I), mink enteritis virus (MEV) and raccoon parvovirus (RPV).[4–8] The nucleotide sequences of the capsid protein genes of FPV and CPV are greater than 98% homologous.[9–12] Genetic recombination indicates that very few changes are required within the coat protein gene region to endow FPV with the ability to replicate in dogs.[6,13] However, both viruses can be distinguished by a number of biological properties, such as host range in vitro and in vivo, antigenicity and by the conditions required for hemagglutination.[6,12,13] These differences have been mapped to the amino acid changes between FPV and CPV in the coat protein[6,12,13] (Table I; Fig. 1).

The three-dimensional structures of full and empty CPV particles have been determined to atomic resolution using X-ray crystallography.[14–16] The structure consists of 60 copies of the capsid protein arranged with icosahedral symmetry. The polypeptide fold contains the same eight-stranded antiparallel β-barrel motif as has been observed in most other known icosahedral viruses that infect eukaryotes.[17] However, two-thirds of the structure is the

Received July 30, 1992; revision accepted January 25, 1993.

Address reprint requests to Dr. Michael G. Rossmann, Department of Biological Sciences, 1392 Lilly Hall of Life Sciences, Purdue University, West Lafayette, IN 47907-1392.

TABLE I. Amino Acid Differences Between FPV and CPV

	Amino acid sequence number									
	80	93	103	232	323	375	386	484	564	568
CPV	R	N	A	I	N	N	K	V	S	G
FPV	K	K	V	V	D	D	Q	I	N	A
Position on FPV structure*	B Loop 1	S Loop 1	B Loop 1	S Loop 2	S Loop 3	B Loops 3–4	S Loops 3–4	B Loop 4	S C-terminal	B C-terminal

*Position on FPV structure (see Fig. 1) shows buried (B) and surface accessible (S) residues.

result of insertions between the strands of the β-barrel. These insertions form elaborate loops on the surface of the virus, the most prominent of which is the 22 Å long spike on the 3-fold axes. There is a 15 Å canyon-like depression circulating around each of the 5-fold axes and a dimple-like depression at the 2-fold axes. The amino acids which differ between FPV and CPV cluster around the rim of the 2-fold dimple-like depression (Fig. 1). The canyon-like depression and the dimple are postulated as possible sites of host cell receptor attachment by analogy to picornaviruses.[17,18] Residue 93, which has been found to be associated with host range differentiation between FPV and CPV and a CPV specific epitope, is found on the threefold spike. This study of the three-dimensional structure of FPV was undertaken in an effort to elucidate the roles of structural modifications in the biological differentiation between FPV and CPV.

Viral structure determination is dependent upon the use of noncrystallographic symmetry for refinement and extension of phases.[19] Initial phases to low resolution may be obtained by isomorphous replacement, as was the case with the structure determinations of human rhinovirus 14,[17] poliovirus,[20] and black beetle virus,[21] or by the use of an atomic model of a solved structure, as for Mengo virus,[22] human rhinovirus 1A,[23] foot-and-mouth disease virus,[24] and the bacteriophage ϕX174.[25] The structure of a CPV full particle[14,15] was used as an initial model in the structure determination of the orthorhombic form of FPV empty particles.

CRYSTAL PREPARATION AND DATA HANDLING

The FPV virus particles were propagated in monolayers of NLFK feline kidney-derived cells,[26] grown in 50% McCoy's 5A and 50% Leibovitz L15 media with 5% fetal bovine serum. The virus purification involved 3 cycles of freezing and thawing, followed by polyethylene glycol (PEG) 8000 precipitation. The precipitate was then chloroform extracted (twice), followed by two cycles of linear sucrose gradient (10–40%) purification. The empty and full particles (70 S and 110 S, respectively) were collected and used for crystallization, after dialysis against 10 mM Tris-HCl (pH 7.5) and concentration to 10 mg/ml by ultracentrifugation. Crystallization of purified virus particles was achieved using the hanging drop vapor diffusion method.[27] Useful crystals were obtained for both full and empty particles at room temperature, with PEG 8000 as the precipitant. The reservoir solution contained 0.75% (w/v) PEG 8000 and 8 mM $CaCl_2$ in 10 mM Tris-HCl (pH 7.5) buffer, over which was suspended a hanging drop of 5 μl of virus diluted by 5 μl of the reservoir solution. Crystals grew in a period of 2 weeks or longer (Fig. 2). Various crystal forms, which were not distinguishable morphologically, were obtained for both full and empty particles, resulting in random data collection for the various crystal forms (Table II). We report here the structure determination of the orthorhombic crystal form of FPV empty particles.

The X-ray diffraction data collection was by oscillation photography (Fig. 3), using both the A1 and F1 stations at the Cornell High Energy Synchrotron Source (CHESS). No attempt was made to align the crystals optically and no "setting photographs" were taken in order to avoid possible radiation damage following initial exposure. Two to 40 photographs per crystal (depending on crystal size) were obtained using a 0.4° oscillation angle, while cooling to 4.0°C. The diffraction patterns extended to about 2.8 Å resolution. The films were indexed using Kim's autoindexing procedure,[28] processed[29] to 3.0 Å resolution, scaled together, and post-refined[30] assuming orthorhombic symmetry, to give 45% of all possible data (Table III). The primitive cell dimensions were found to be a = 380.1 Å, b = 379.3 Å, and c = 350.9 Å. The crystal system was confirmed by the good agreement between orthorhombic symmetry related structure amplitudes. The cell dimensions for a and b were very similar, but tetragonal symmetry was eliminated because of the absence of 4-fold symmetry. Due to the similarity between the a and b cell dimensions, films were indexed and processed using both axial assignments. The data were then scaled to a standard initial single crystal data set of 20 films to determine the same indexing convention. This procedure was used for data from each new crystal, before being combined to the current processed data set. The space group $P2_12_12_1$ was assigned on the basis of systematic absences along the axial reflections. With 4 particles per unit cell, V_M was calculated to be 3.0 $Å^3$/Da,[31] showing that there

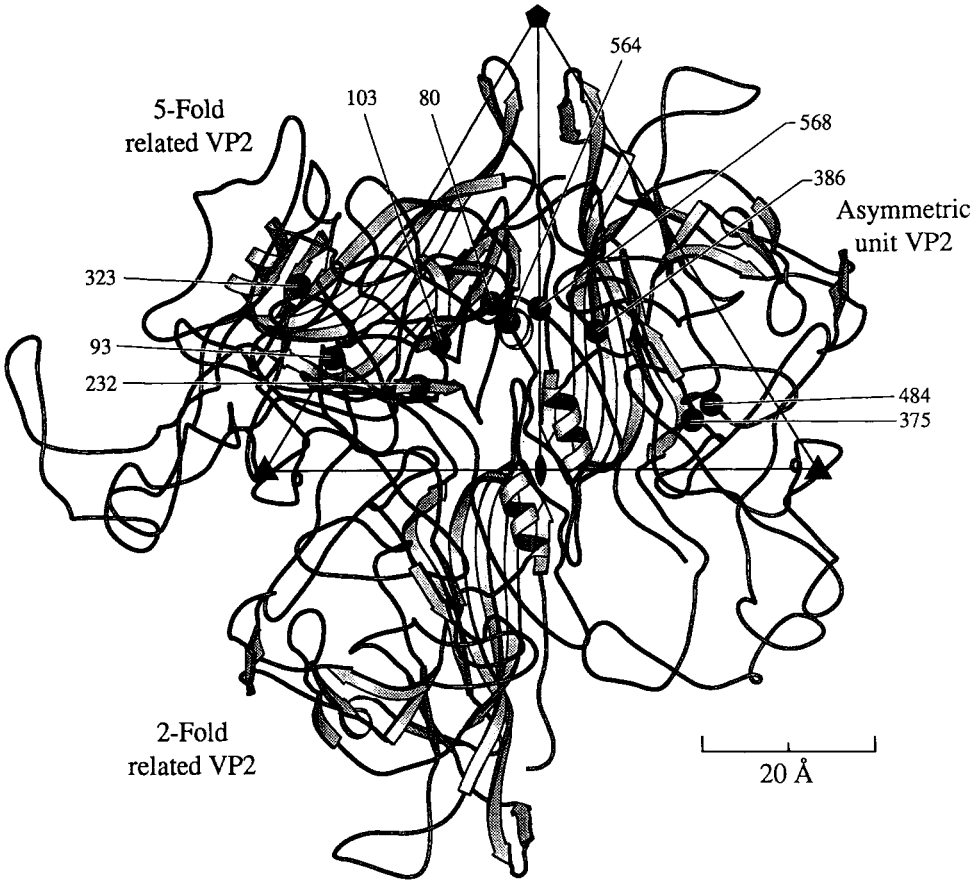

Fig. 1. Ribbon diagram showing the secondary structure of FPV and the location of amino acid differences to CPV (stippled circles). The orientation of VP-2 is shown, viewed down a 2-fold axis relative to an icosahedral asymmetric unit formed by adjacent 5-, 3-, and 2-fold axes. Fivefold and 2-fold related VP-2 capsid proteins are also shown.

was one virus particle per asymmetric unit, resulting in 60-fold noncrystallographic redundancy per crystallographic asymmetric unit.

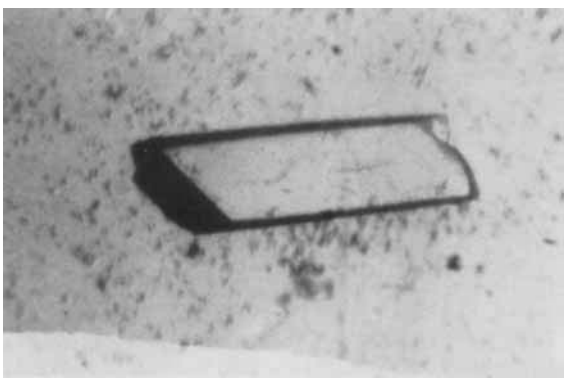

Fig. 2. Optical micrograph of a crystal, about 1 mm long, of FPV empty particles.

THE ORIENTATIONS AND POSITIONS OF THE PARTICLES

It is convenient to define two types of unit cells before describing the procedures used in molecular replacement. The "p-cell" is the unit cell of the unknown crystal structure with an orthogonalized coordinate system, **Y**, in this case the orthorhombic $P2_12_12_1$ cell of FPV. The "h-cell" is the unit cell containing a single particle in a known standard orientation (Fig. 4A) and has a Cartesian coordinate system, **X**. A matrix, [**P**], defines a rotational relationship between the structures in the h-cell and the reference particle in the p-cell,[32] so that $\mathbf{X} = [\mathbf{P}]\,\mathbf{Y}$.

The orientations of the virus particles in the unit cell were determined using a self-rotation function.[33] The initial orientation was calculated using data between 10.0 and 7.0 Å resolution. The function was explored in the spherical polar coordinates in 2° intervals, to search for 2-fold ($\kappa = 180°$), 3-fold ($\kappa = 120°$), and 5-fold ($\kappa = 72°$ or 144°) noncrystallographic axes (Fig. 4B). The self-rotation function

TABLE II. Crystal Forms of FPV Full and Empty Particles

Space groups	Cell parameters	Particles per asymmetric unit
FPV monoclinic $P2_1$ (I)	$a=382.9$ Å, $b=252.2$ Å, $c=266.8$ Å, $\beta=94.2°$	1
FPV* monoclinic $P2_1$ (II)	$a=266.7$ Å, $b=348.9$ Å, $c=269.7$ Å, $\beta=90.9°$	1
FPV† orthorhombic $P2_12_12_1$ (I)	$a=380.1$ Å, $b=379.3$ Å, $c=350.9$ Å	1
FPV orthorhombic $P2_12_12$ (II)	$a=392.5$ Å, $b=275.4$ Å, $c=268.2$ Å	1/2

*Isomorphous with CPV full and empty monoclinic $P2_1$ crystals.
†Data set for empty particles used in this structure determination.

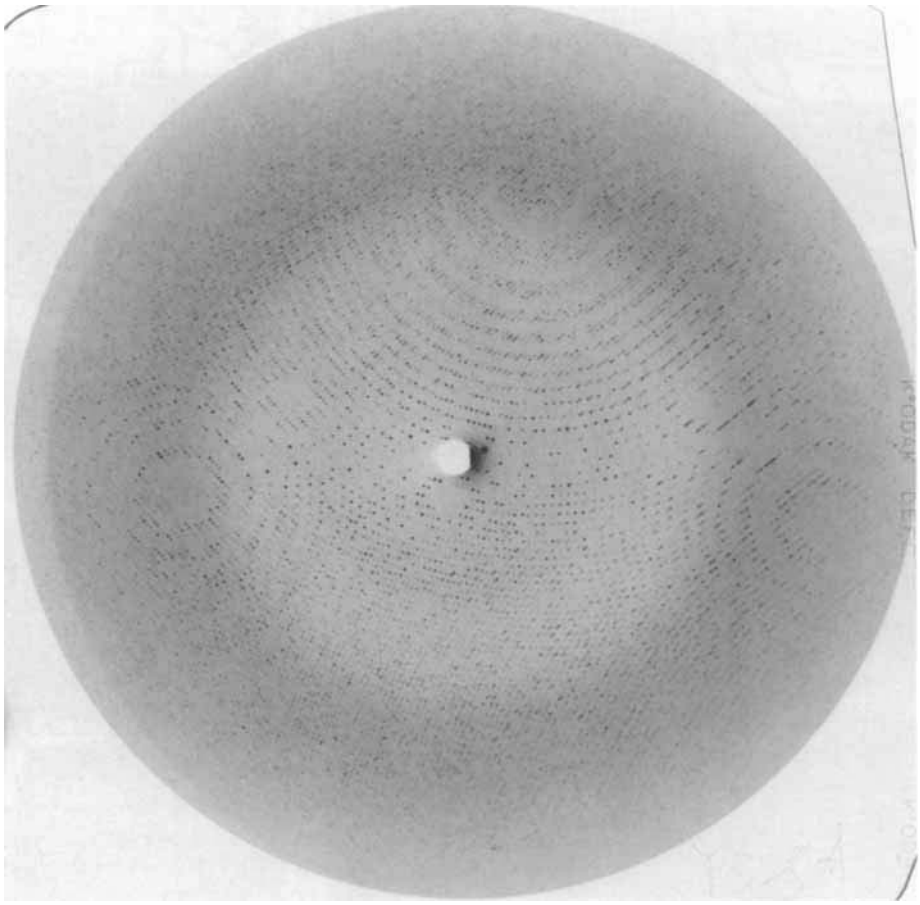

Fig. 3. X-ray diffraction pattern of FPV empty particles in the orthorhombic crystal form taken at the Cornell High Energy Synchrotron Source (CHESS) using a wavelength of $\lambda = 0.91$ Å and an exposure time of 30 sec with an oscillation angle of 0.4°.

was calculated using a partial data set which was 44% complete to 7.0 Å resolution, of which 12% of the largest terms were used to represent the second Patterson.[34] The radius of integration was 120.0 Å and the interpolation grid around each rotated non-integral reciprocal lattice point was 3 × 3 × 3. The somewhat special orientation of the particle in the asymmetric unit gave overlap between peaks from crystallographically related icosahedra. A self-rotation function using data between 4.0 and 3.0 Å resolution gave rise to 4 unique particle orientations in the crystal cell. One of the four solutions was selected (Fig. 4C) and its 60 icosahedral symmetry elements refined by a least-squares procedure[35] against a set of ideal icosahedral vectors in the standard orientation of the h-cell. This standard orientation was defined as shown in Figure 4A. The high resolution observed positions of the icosahedral sym-

TABLE III. The Final Percentage of Data in Each Resolution Shell Collected for Orthorhombic Crystals of FPV Empty Particles

	Resolution (Å)											Overall	Overall
	35–20.0	20.0–8.0	8.0–6.0	6.0–5.0	5.0–4.5	4.5–4.0	4.0–3.7	3.7–3.5	3.5–3.3	3.3–3.2	3.2–3.0	% of data	R_{merge}* (%)
% of data with $I/\sigma(I) \geq 2$	69	85	80	78	78	74	68	62	56	43	35	45.3	14.6

*$R_{merge} = \frac{\sum_h \sum_i (I_h - I_{hi})}{\sum_h \sum_i I_h} \times 100$ where I_h is the mean of the i intensity observation, I_{hi}, for reflection h.

metry axes had an angular rms deviation of 0.05° from that of a geometrically ideal icosahedron, corresponding to a distance of 0.1 Å at a radius of 120.0 Å. The results of the self-rotation function were confirmed by a locked-rotation function[36] using the same parameter settings and approximately 1% of the data as large terms. The final results of the rotation function showed that

$$[\mathbf{P}] = \begin{pmatrix} 0.9676 & 0.1972 & -0.1578 \\ -0.1614 & 0.9634 & 0.2141 \\ 0.1943 & -0.1817 & 0.9640 \end{pmatrix}.$$

This represents a rotation of 18.65° of the standard icosahedron (Fig. 4A) about an axis whose direction cosines are (0.6189, −0.5505, −0.5604) with respect to the orthogonal crystal axes.

To initiate phasing of the FPV empty orthorhombic structure factors, the CPV full monoclinic structure[14,15] was used as a starting model. Using a 6.0 Å resolution electron density map of the monoclinic CPV full structure, a single CPV particle was placed in an h-cell by averaging and skewing the map. This type of averaging, given 60-fold redundancy, essentially cancels out all other particles that do not obey the local noncrystallographic symmetry with respect to the chosen particle center. Structure factors were then calculated from this CPV h-cell map by Fourier inversion. The calculated h-cell structure factors were used for a cross-rotation function with respect to observed structure factors of the FPV empty particle diffraction data. The results (Fig. 5) showed that there was excellent correspondence.

Inspection of the space group diagram for $P2_12_12_1$ shows that there will be least overlap between four spherically shaped molecules in the unit cell if their centers are at $(\frac{1}{4}, \frac{1}{4}, \frac{1}{4})$ or $(\frac{1}{2}, \frac{1}{2}, \frac{1}{2})$. To determine the particle position, the structure factors derived from the CPV model in the h-cell were used in a translation function R-factor search, based on the knowledge of the particle orientation in the p-cell.[37] Using all data between 15.0 and 6.0 Å of a partial data set (68% complete to 6.0 Å), with a grid step size of 0.04 Å and a radius of integration of 120.0 Å, a minimum was observed at 0.4976, 0.5209, 0.5029, with an R-factor of 31.4% (Fig. 6).

PHASE EXTENSION BY MOLECULAR REPLACEMENT FROM 6.0 Å TO 3.3 Å RESOLUTION

Phases were generated between 15.0 and 6.0 Å resolution using the CPV model, given the known particle orientations and centers in the FPV unit cell. Higher resolution phases were not used in an effort to avoid undue bias from the CPV model. Phase improvement followed using 6 cycles of 60-fold icosahedral symmetry averaging and solvent flattening.[19,32] A spherical shell envelope was defined with an outer radius of 140.0 Å and an inner radius of 75.0 Å. A tangential plane was used to separate particles, where there was overlap between spheres. All the points defined in the protein region were 60-fold averaged; points less than the inner radius and those outside the outer radii were set to a mean of all the solvent densities, which was close to zero. Calculated structure factors were not used to supplement the 68% of observed structure factors to 6.0 Å resolution. The mean correlation coefficient improved from an initial value of 0.74 to 0.84 (Fig. 7). At this point the reference particle orientation was redetermined using higher resolution data (4.0–3.0 Å) and an improved [P] matrix was found (see above). A further cycle of averaging with this new [P] matrix resulted in an improvement of the correlation coefficient by 0.03 in all resolution shells.

Phase extension was carried out one reciprocal lattice point at a time to 5.4 Å resolution, with four cycles of averaging at each extension. At this stage the reference particle position was refined using a newly generated h-cell derived from the averaged FPV density. A slight positional change (0.05 Å) was found with resultant coordinates of 0.4977, 0.5208, and 0.5029. It was assumed, therefore, that no significant improvement could be obtained in the particle position at later stages of phase extension.

After phase extension to 5.2 Å resolution, a true molecular envelope was generated with limiting outer and inner radii of 140.0 and 75.0 Å which underwent hole-filling and symmetrization.[32,38] On implementing this envelope there was no significant improvement in the correlation coefficients or increase in phase convergence. However, the envelope

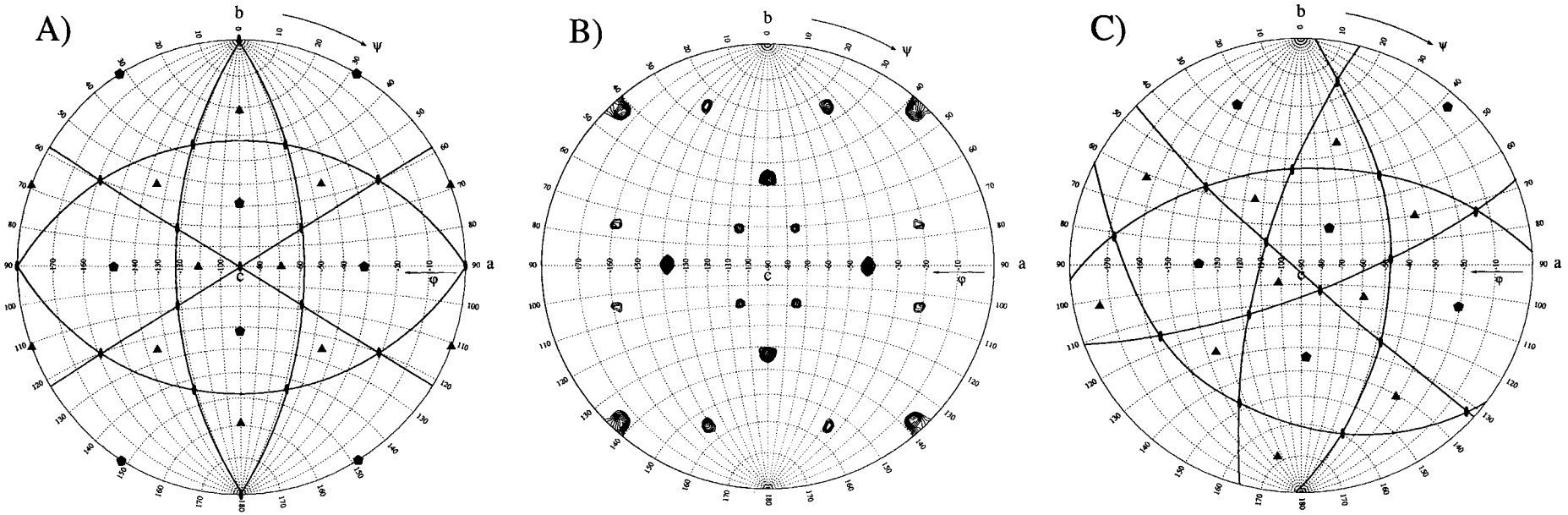

Fig. 4. (**A**) Definition of the standard icosahedral orientation (as defined in the h-cell). Three mutually perpendicular 2-fold axes are parallel to *a*, *b*, and *c*. (**B**) Rotation function, for $\kappa = 72°$, for FPV empty particles in the orthorhombic crystal form using a 10.0–7.0 Å resolution partial data set that contained approximately 44% of the observable data. (**C**) The symbolic interpretation of the complete rotation function ($\kappa = 72°$, 120°, and 180°) for one of the four particles in the unit cell. Great circles pass through the 2-fold axes of the single particle orientation.

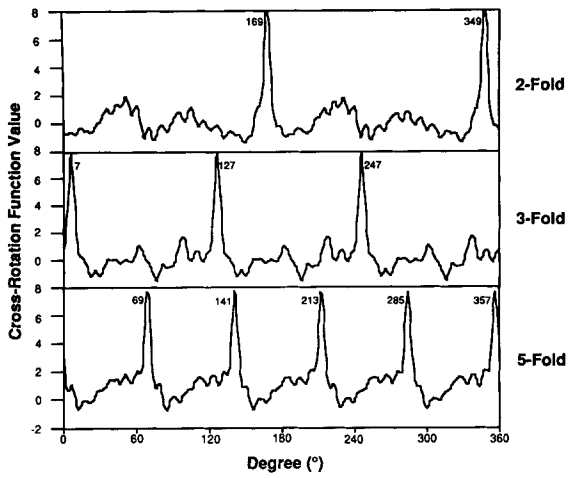

Fig. 5. The cross-rotation function between the h-cell CPV full particles and the FPV empty particles in the orthorhombic crystal form. A selected 2-, 3-, or 5-fold axis of CPV in the h-cell was superimposed on a corresponding 2-, 3-, or 5-fold axis of FPV in the orthorhombic cell. The CPV structure was rotated in 1° intervals about the common superimposed axes. The function was calculated using data between 15.0 and 10.0 Å resolution.

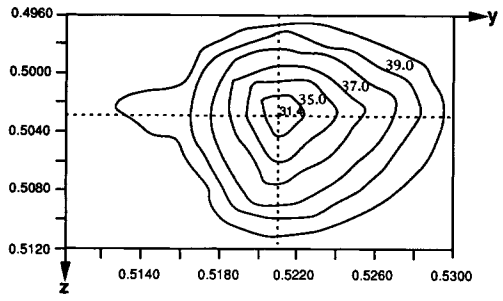

Fig. 6. Plot of *R*-factors (%) in section $x = 0.4976$ to establish the particle position using the correctly oriented CPV model with 15.0–6.0 Å resolution data. The *R*-factors are defined as

$$R-\text{factor} = \frac{\sum||(|F_{obs}| - k|F_{cal}|)|}{\sum|F_{obs}|} \times 100.$$

had the computational benefit of reducing the number of points being averaged by approximately 30% in the exterior solvent region, allowing more grid points to be solvent flattened, thus speeding up the turnover time for each cycle of real space averaging (Table IV).

Phase extension continued to 3.3 Å to give a final mean correlation coefficient of 0.79 (Fig. 7). The total procedure required 45 steps of increasing reciprocal lattice points sequentially and approximately 260 cycles of averaging. A new molecular envelope was generated whenever the electron density map sampling became too coarse. Sampling was maintained at approximately 1/3 of the map resolution and the electron density was interpolated using eight surrounding points. At various times in the

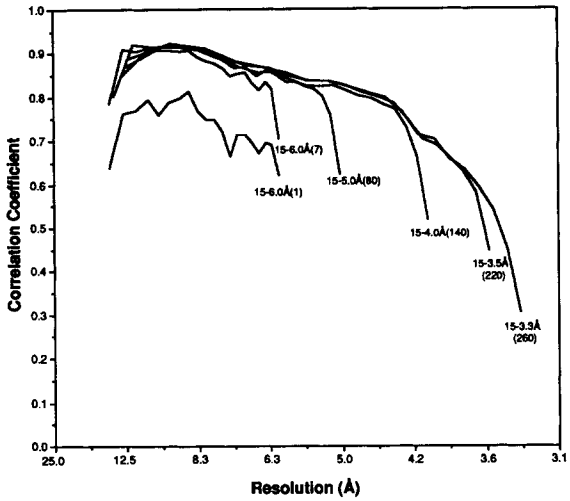

Fig. 7. A plot of correlation coefficients, *C*, against resolution during molecular averaging and phase extension of FPV empty particles in the orthorhombic cell. The correlation coefficient is defined as

$$C = \frac{\sum(\langle F_{obs}\rangle - F_{obs})(\langle F_{cal}\rangle - F_{cal})}{[\sum(\langle F_{obs}\rangle - F_{obs})^2 \sum(\langle F_{cal}\rangle - F_{cal})^2]^{1/2}}$$

Correlation coefficients are shown for (i) after the first cycle of molecular averaging (15.0–6.0 Å), (ii) after seven cycles of phase improvement (15.0–6.0 Å), (iii) after 80 cycles of phase extension and improvement (15.0–5.0 Å), (iv) after 140 cycles of phase extension and improvement (15.0–4.0 Å), (v) after 220 cycles of phase extension and improvement (15.0–3.5 Å), (vi) after 260 cycles of phase extension and improvement (15.0–3.3 Å). The cycle number is shown in parentheses.

phase extension procedure additional observed structure factors were included as more data became available, resulting in slight increases in correlation coefficients. Attempts were made at several resolution limits to include calculated structure factors in place of unobserved reflections, but surprisingly a decrease in the mean correlation coefficient was always observed. Thus, calculated structure factors were never included.

The real space averaging calculations[32] were carried out on a Cyber205, an IBM RISC 6000 workstation model 540 and an Intel 1860 Hypercube. Table V gives examples of executable times for these machines for two maps at the same resolution and grid sampling.

RESULTS

The electron density map obtained for the FPV empty particles was readily interpreted in terms of the amino acid sequence of the FPV VP-2 protein (Fig. 8). The VP-2 polypeptide trace was very similar to that observed for the CPV structure and is shown in Figure 9. The surface topology of both viruses are shown in Figure 10. As with CPV, the first 37 residues of the FPV VP-2 were disordered and none of the amino acids in the VP-1 unique amino terminus was observed. However, as in the electron

TABLE IV. Statistics Comparing the Spherical and Molecular Mask Used in Real Space Electron Density Averaging

	Spherical mask	Molecular mask
Resolution range (Å)	6.0–5.2	5.2–3.8
Number of grid points along *a, b, c*	280, 280, 260	280, 280, 260
Limiting external and internal radii (Å)	140.0 and 75.0	140.0 and 75.0
% of points within mask	72.8	45.7
% of solvent points outside particle	13.1	40.1
% of solvent points inside particle	14.1	14.2

TABLE V. Comparison of Execution Times in CPU Minutes for One Cycle of Real Space Molecular Averaging Program on Various Computers

Computer	At a resolution of 3.5 Å using a unit cell grid size of 320, 320, 300	At a resolution of 3.3 Å using a unit cell grid size of 340, 340, 320
Intel 1860 Hypercube (8 nodes)*	140	193
IBM RISC 6000	464	579
Cyber205	162	194

*Additional improvements to the program now reduce these times by a factor of 2.5.

density for the CPV full particles, there is electron density extending along the 5-fold axes, although it is not connected to residue 38 at the base of the 5-fold cylindrical structure. An indication that the phases were not biased toward the CPV full particle starting model was the absence of the DNA density seen in the CPV full particle electron density map.[14,15] The FPV model was built on an Evans & Sutherland PS390, using the interactive program FRODO.[39,40] The unrefined coordinates have been deposited with the Brookhaven Protein Data Bank.

The initial atomic model of the FPV structure was built into the density using the unrefined atomic coordinates of CPV full particles after replacing the side chains for those amino acids that differed between the two viruses (Table I) and deleting the DNA. Residues appropriate to FPV could be clearly differentiated to those that exist in CPV. This was exemplified by the observation of a Lys side chain at residue 93 in loop 1 (Fig. 11A), where there is an Asn in CPV (Fig. 11B).

Side chain and sometimes main chain conformational differences between FPV and CPV were observed in the regions proximal to the amino acid changes. The largest structural differences (up to 7 Å in atomic displacement) occurred between residues 224 and 228 at the top of loop 2 (Fig. 12A), residues 358 to 374 between loop 3 and loop 4 (Table VI; Fig. 12B) and at the region corresponding to the DNA interactions in CPV full particles (Fig. 13). None of these differences can be attributed to lattice contacts as there are 60 different types of contacts associated with each particle. If the lattice contacts had been the cause of the conformational changes, then these should result in many different conformations which could be averaged out and become uninterpretable in the map.

The conformational changes at the top of loop 2 from residue 224 to 228 are associated with the change in loop 1 of N93 in CPV to K93 in FPV. Residue N93 in CPV is partially covered by the top of loop 2 and its side chain points toward the interior of the virus (Fig. 12A). In contrast, in FPV K93 points outward toward loop 2 where there are hydrogen bonds between the lysine's amino group and the carbonyl oxygens of residues 225 and 227 (Fig. 12A). K93 is much more exposed on the surface of the FPV capsid than is N93 on the CPV capsid (Figs. 12A and 14B), and loop 2 has moved away to accommodate the lysine in FPV (Fig. 12A). The changes at the tops of loop 1 and loop 2 are transmitted to adjacent residues, between 80 to 96 and 219 to 236, respectively. In addition, there appear to be other smaller changes in this region, less than 1 Å, whose significance cannot be assessed without crystallographic refinement.

In the region between residues 358 and 374 the FPV polypeptide follows a completely different path in comparison to that observed in both the CPV full[14,15] and empty[16] particle structures (Figs. 9 and 12B). In both the CPV structures the low density shows this loop to be slightly disordered, whereas in the FPV structure the altered conformation is of high density and, therefore, well ordered. The residues of this loop are located on the wall of the 2-fold depression. The nearest FPV-CPV amino acid differences to this region are at residues 375 and 323 in the 3-fold related subunits (Fig. 14) both of which change from Asn in CPV to Asp in FPV. Residue D375 is associated with a small loop in FPV (371 to 374) which has an extended conformation in CPV (Fig. 12B). This small loop appears to be stabilized by a putative cation which is liganded by carboxy groups from residues 368, 373, and 375. The exposed surface area of the 358–374 loop is much less in FPV than in CPV (Fig. 14) as a result of the burial of residues 361, 364, 369, and 370.

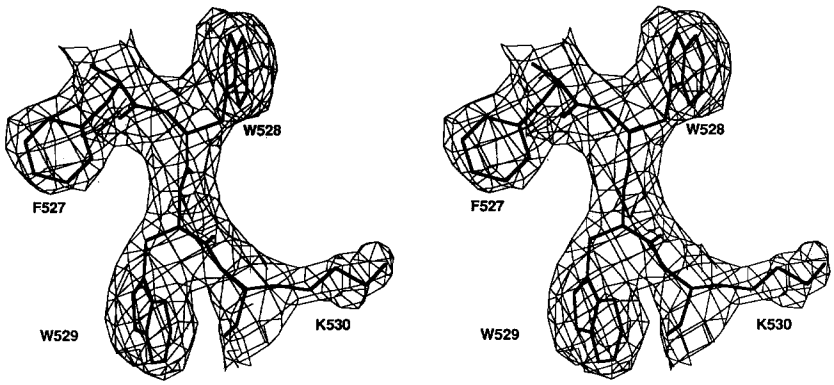

Fig. 8. A piece of electron density showing amino acids 527 to 530.

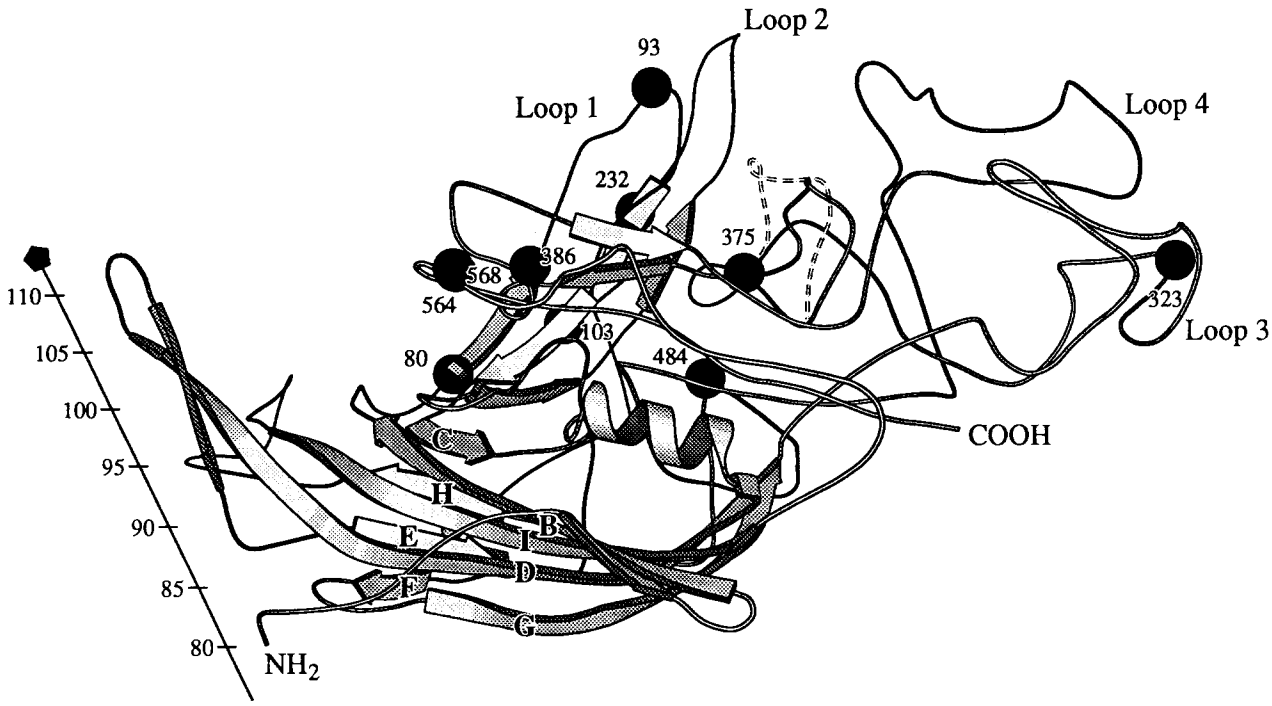

Fig. 9. A ribbon diagram of the VP-2 topology of FPV showing its secondary structure. The dotted line represents the conformation of the CPV loop between residues 358 to 374. Shown also are the positions of the 10 amino acids that differ between the two viruses (stippled balls). The nearest 5-fold axis is shown with radial distances from the viral center in Å.

The structure of CPV full particles shows some systematic binding of DNA to the inside protein shell.[14,15] In the FPV empty capsid structure the side chains of the amino acids, and in some regions the main chain atoms, occupy a portion of the space created by the absence of DNA (Fig. 13). The structures of CPV empty particles[16] and FPV empty particles are very similar in this respect.

THE BIOLOGICAL SIGNIFICANCE OF THE OBSERVED STRUCTURAL DIFFERENCES BETWEEN FPV AND CPV

Host Range

Host range differentiation between viruses might occur at various stages of the virus' life cycle, including cell receptor attachment, viral entry, uncoating,

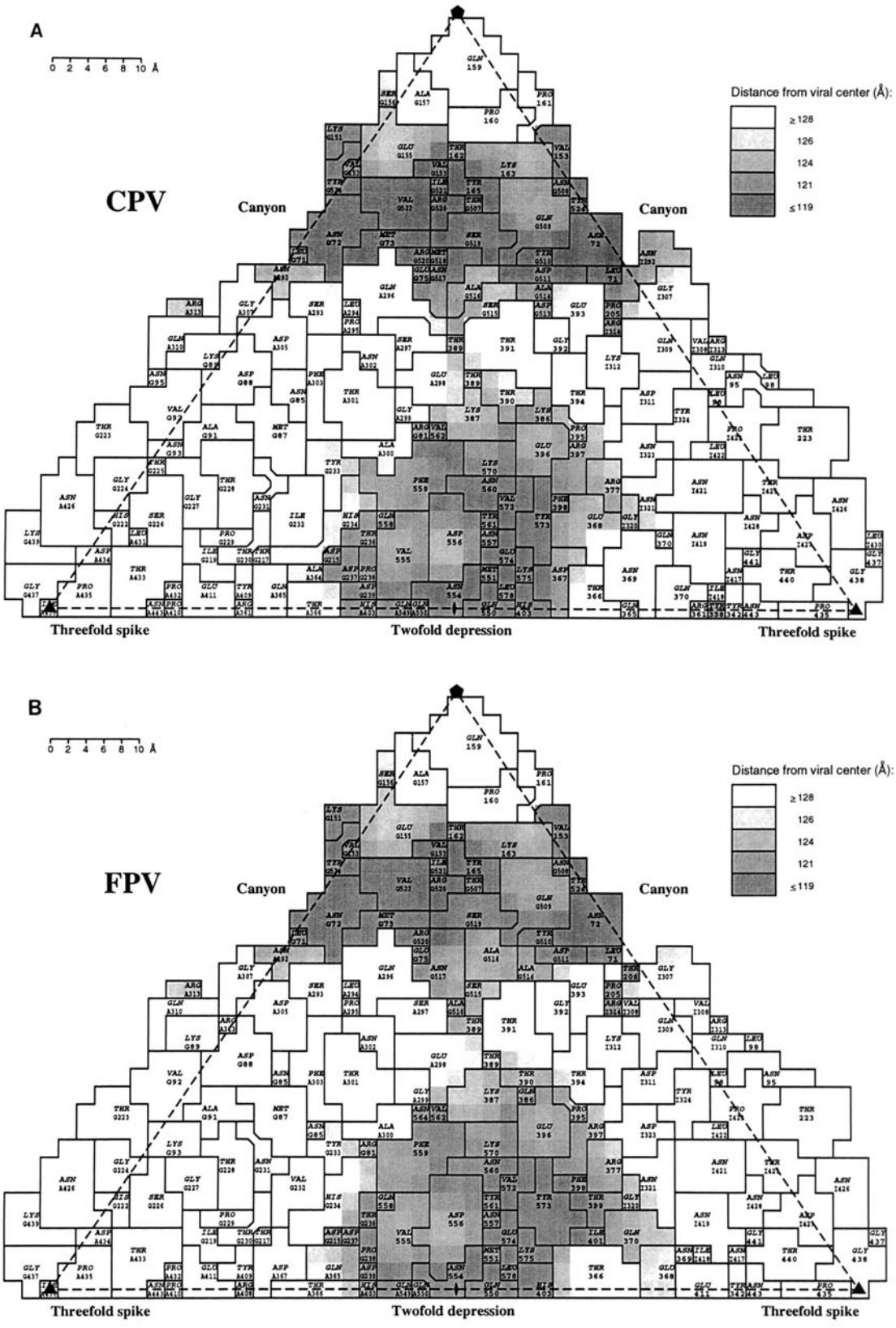

Fig. 10. (**A**) Two-dimensional "road map" of the residues that compose the CPV surface within one icosahedral asymmetric unit. The canyon, 3-fold spike and the 2-fold dimple depression are labeled. (**B**) Two-dimensional "road map" of the residues that compose the FPV surface within one icosahedral asymmetric unit. The canyon, 3-fold spike and the 2-fold dimple depression are labeled. Letters in front of the sequence numbers indicate the symmetry operations used to generate the residue from the reference subunit. Absence of such a letter shows that the residue belongs to the reference subunit. "A" is a 2-fold operation, "G" is a clockwise 5-fold operation and "I" is a clockwise 3-fold operation with respect to the 3-fold axis at the bottom right of the diagram.

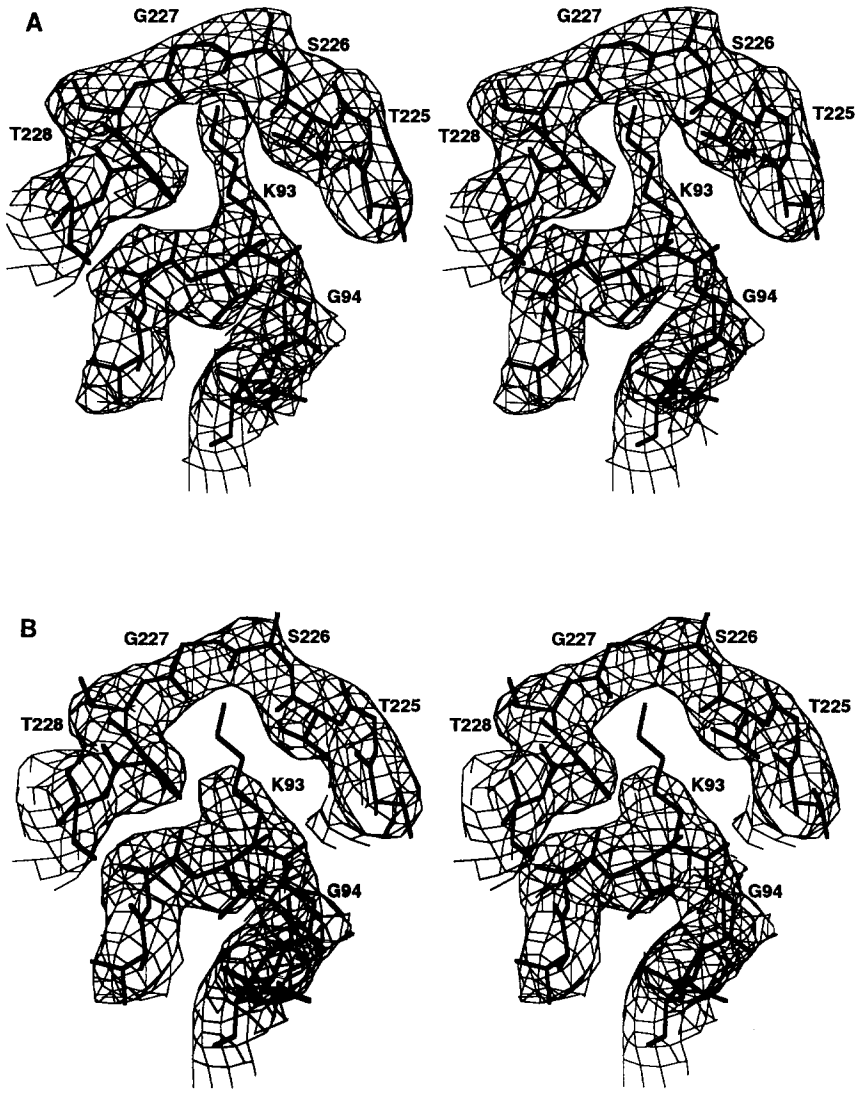

Fig. 11. A stick diagram of FPV loop 1 (residues 90 to 94) and loop 2 (residues 224 to 229) superimposed on the electron density of (**A**) FPV and (**B**) CPV.

DNA replication, or transcription. While CPV can replicate in dogs or dog cell cultures and FPV can replicate in cats and cat cell cultures, there is an apparent difference in the ability of CPV to replicate in cats or cat cell cultures and FPV to replicate in dogs or dog cell cultures (Table VII).[41] Host range differentiation between FPV and CPV is likely to be at an early stage of infection because dog cells transfected with FPV DNA, thus bypassing cell recognition and uncoating, can produce infectious virus.[42] On the other hand, studies with two strains of minute virus of mice (MVM; a parvovirus) indicate that tissue tropism is determined by events occurring after the external receptor binding, but relate to inhibition of viral DNA replication.[43] The only known nucleotide changes between FPV and CPV which affect CPV host range (but not necessarily FPV host range) correspond to residues 93, 103, and 323.[13] These residues are on the elaborate loops which make up the 3-fold spikes on the virus surface (Fig. 10), although only residues 93 and 323 (Fig. 14) are surface accessible. Both these residues are associated with the largest structural differences between FPV and CPV (Figs. 11 and 14). Hence, if host range is associated with receptor interaction, then the receptor attachment site on CPV would be expected to straddle these two residues (Fig. 14). Residues equivalent to 316 and 320 in CPV[8] have been implicated in MVM tissue tropism.[44] These two residues are on or near the surface and are in the gen-

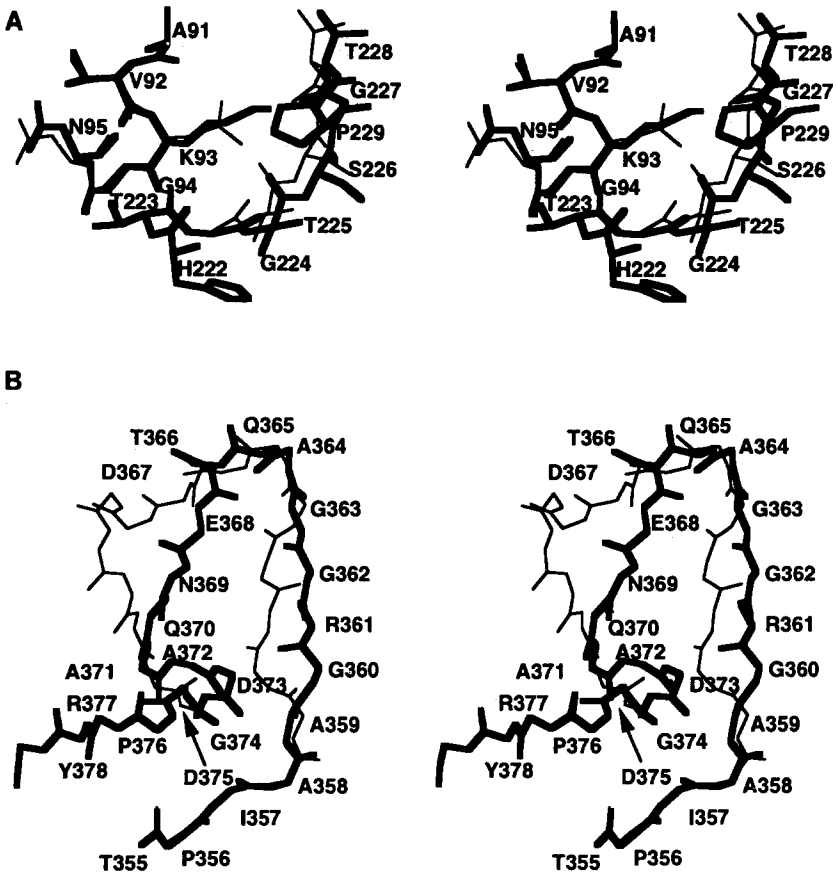

Fig. 12. (**A**) A stick representation of the conformational change between the FPV and CPV structures at the top of loop 1, showing residues 91 to 94, and the top of loop 2, showing residues 222 to 228. The FPV residues are shown in bold and are labeled. The diagram is viewed in the same orientation as in Figure 10. (**B**) A stick representation of the conformational change between the FPV and CPV structures at residues 355–378. The side chains of the amino acids are omitted for clarity. The FPV residues are shown in bold and are labeled.

TABLE VI. C_α Movement in Loop 357–375 Between the CPV and FPV Structures

Residue	357	358	359	360	361	362	363	364	365	366	367	368	369	370	371	372	373	374	375
Distance* (Å)	0.2	0.3	0.8	3.9	2.5	4.9	3.7	0.9	4.9	0.8	6.6	6.8	7.1	4.7	5.8	5.0	4.5	0.5	0.0

*The distance is calculated as the change in position of the C_α coordinates for each residue.

eral area of the putative receptor binding attachment site for CPV (Fig. 14) defined by residues 93 and 323.

Antigenicity

A series of neutralizing antibodies have been selected against both CPV and FPV.[45] Many, but not all, of the CPV neutralizing antibodies also neutralize FPV and similarly many, but not all, of the FPV antibodies neutralize CPV. Further selection of escape mutations shows that the antibodies bind to two distinct epitopes, A (associated with mutations at residues 93, 222, 224, and 426) and B (associated with escape mutations at residues 299, 300, 302, and 305)[46] (Fig. 14). ELISA binding studies[46] and hemagglutination inhibition studies[13] show that the escape mutations are associated with inability to bind neutralizing antibodies. Both epitopes A and B are on the elaborate loops forming the 3-fold spikes. A change of CPV N93 to FPV K93 is seen to cause a major conformational change in epitope A (Figs. 12A and 14). As in picornaviruses, the neutralizing epitopes are on highly exposed regions of the virus capsid.[17] Furthermore, comparison of related parvoviruses shows this region to be among the most variable regions of VP-2.[8] The two major neutralizing epitopes A and B correspond to two of the 10 antigenic binding sites on the surface of CPV deter-

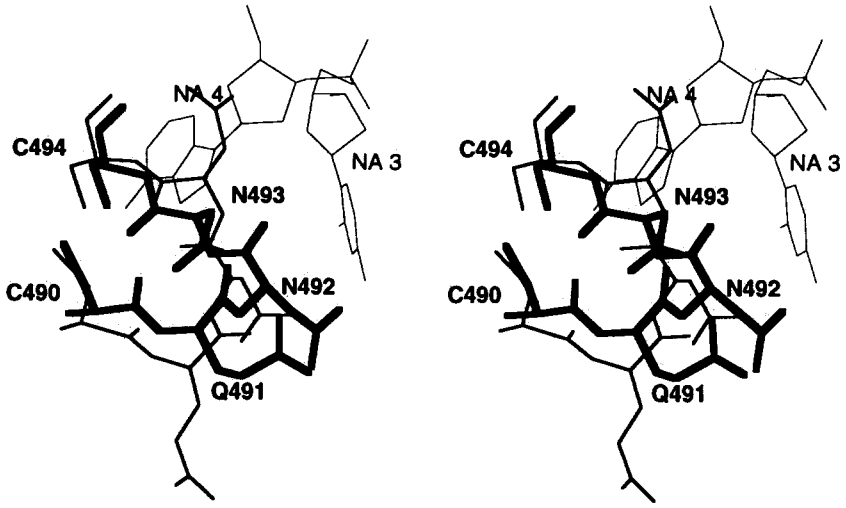

Fig. 13. A stick representation of some of the conformational changes between CPV full and FPV empty particles showing residues 490–494 near the binding site of ordered DNA. The FPV residues are shown in bold and are labeled, while CPV is given in medium thickness and the nucleic acid in thinnest lines.

mined by using nonapeptides of the VP-2 sequence in an automated pepscan procedure.[47] Presumably some of the remaining sites bind antibody but the virus is not neutralized. As is usual for mapping neutralizing sites with antibody escape mutations,[46] the reason for the inability of a particular escape mutant to bind antibody is not immediately apparent.

Hemagglutination

FPV and CPV can be distinguished by the conditions at which they hemagglutinate Rhesus monkey erythrocytes. CPV hemagglutinates over a wide pH range, while FPV only hemagglutinates at pH values below 6.8.[13] The pH dependence of hemagglutination (HA) of these two viruses are primarily determined by the type of amino acid at residues 323, 375, and 377 (Table VIII).[48] Both 323 and 375 are required to be Asp in order to obtain pH-dependent HA as in FPV.[48] In addition, when CPV residue 377 is changed from Arg to Lys,[48] CPV does not hemagglutinate at any pH. The three residues 323, 375, and 377 are close to each other and are located on the wall of the dimple-like depression around the 2-fold symmetry axes (Figs. 10 and 14).

The FPV crystals used in this structure determination were obtained at a physiological pH of 7.5 and, hence, should represent the nonhemagglutinating conformation. In contrast, the CPV structure determinations[14–16] represent the hemagglutinating condition. The residues involved in determining the HA behavior of FPV and CPV are located close to the largest conformational difference between the FPV and CPV structures that include residues 358 to 374 (Fig. 12B). Presumably the two additional negative charges (at residues 323 and 375) in FPV near the charges on E368, D373, R377, and R397 (Figs. 10B and 14B) result in interactions which cause the difference in conformation between FPV and CPV in the loop region from residue 358 to 374 (Fig. 12B). In CPV N323 is a surface residue which is hydrogen bonded to R377 and to R397 of the 3-fold related VP-2 protein molecule. In FPV, residue D323 forms a salt bridge with residues 377 and 397. Residue 375, which is also an Asp in FPV, is slightly buried beneath the surface of both viruses, but is at the end of the conformationally altered loop (Fig. 12B). Thus, residue D375 cannot be interacting directly with the receptor on erythrocytes, but is most likely involved in interactions which cause the conformational changes required for receptor binding. Treatment of the erythrocytes with neuraminidase prior to the binding experiment eliminates the HA interaction, suggesting that the receptor on the erythrocytes contains sialic acid.[48] However, the binding of these viruses to erythrocytes is different to binding to host cell receptors, and is noninfectious. This is exemplified by the ability of the nonhemagglutinating mutant of CPV, vB1307 (which, therefore, does not bind erythrocytes) to bind to and replicate in dog cells.[48]

DNA–Protein Interactions

In the CPV full structure, a total of 11 nucleic acids were built into a region of electron density in the interior of the capsid that could not be interpreted as part of the VP-2 polypeptide.[14,15] This density is absent, as expected, in the FPV empty and CPV empty particle structures.[14,16] Since the ordered DNA occurred in each of 60 icosahedral asym-

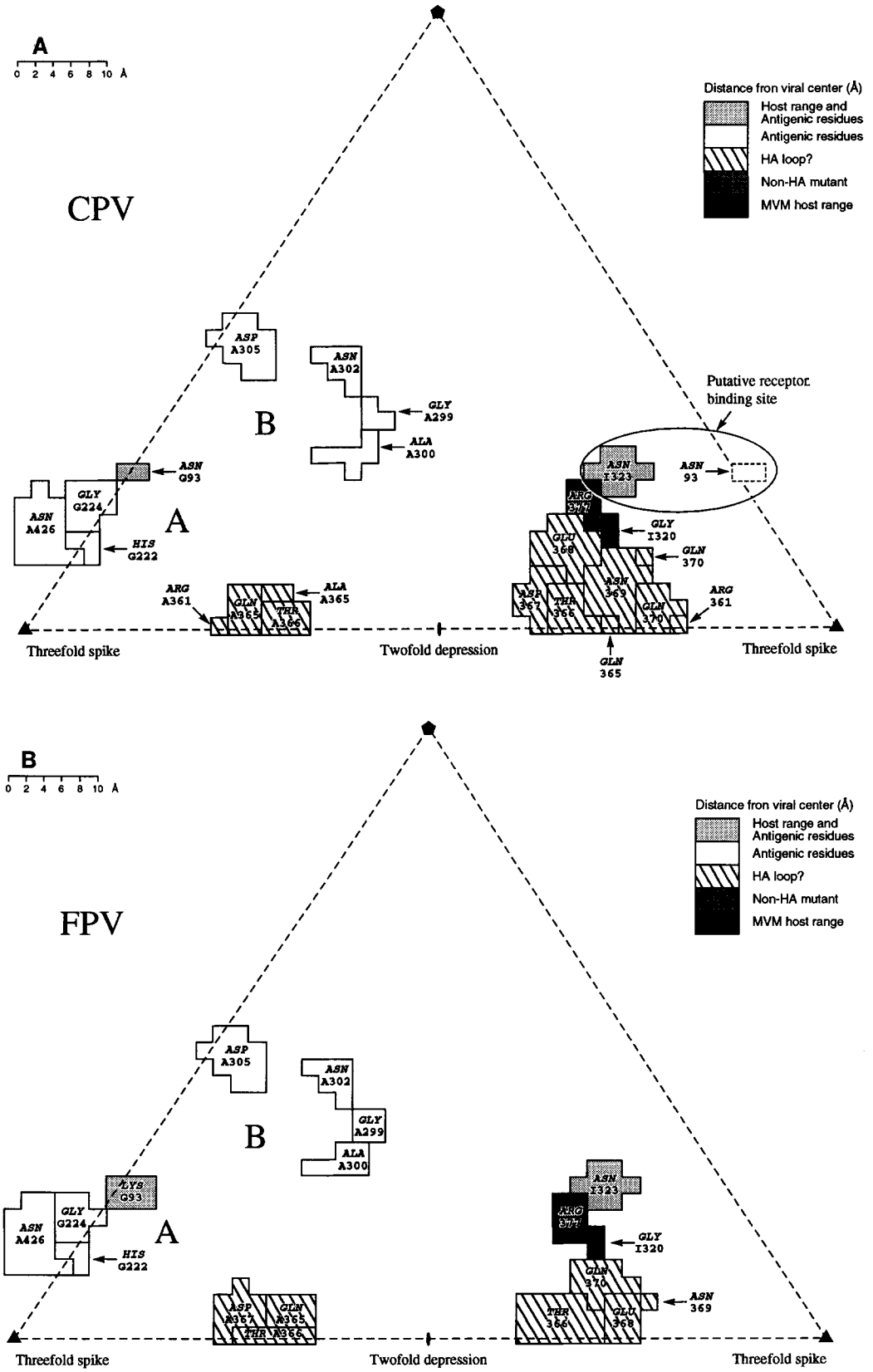

Fig. 14. Two-dimensional "road map" of (**A**) the CPV surface and (**B**) the FPV surface showing residues involved in CPV host range determination, hemagglutination, and antigenicity. The locations of epitopes A and B are also indicated in each panel. In (A), residue 93 from a 3-fold related asymmetric unit is shown within a dashed outline at the putative receptor binding site straddling this residue and residue 323. Both panels (A) and (B) are modified from Figure 10A and B, respectively.

TABLE VII. Host Range of FPV and CPV[13,41]

Host	Ability to infect	
	CPV-2 (wild type)	FPV (wild type)
In vivo		
Cats (most tissues)	−	+
Dogs (thymus and bone marrow)	+	+
Dogs (small intestine and lymph nodes)*	+	−
In vitro		
Most cat cell lines	+	+
Most dog cell lines	+	−

*Target organs for CPV infection.

TABLE VIII. Summary of the Effect of the Residues Determining the pH Dependence of CPV and FPV Hemagglutination*

Virus†	Amino acid at VP-2 residues			Hemagglutination behavior		
	323	375	377	pH-Independent "CPV-like"	pH-Dependent "FPV-like"	Nonhemagglutinating
CPV-d	N	N	R	✓		
vB1307	N	N	K			✓
vB1279	D	N	R	✓		
vB1319	N	D	R	✓		
FPV-b	D	D	R		✓	

*The above results were obtained by modifying residues 323 and 375 in both CPV and FPV. The other differences between CPV and FPV had no major effect on hemagglutinating properties.
†These viruses correspond to those reported in refs. 13 and 48.

TABLE IX. Residues on the Interior of the Capsid Protein in Contact* With DNA

Amino acid residue	DNA base†	Conformational difference between FPV empty and CPV full
F51	Na6, Na7	Yes
K52	Na7	Yes
N56	Na8, Na10	Yes
L177	Na2	Yes
S179	Na2	Yes
N180	Na4, Na6, Na7, Na9	Yes
T182	Na5	Yes
Y244	Na5	No
T263	Na1	No
G264	Na2	No
F266	Na2, Na3	Yes
F267	Na3	Yes
P494	Na2	Yes
G496	Na2	Yes
A541	Na6	Yes
H543	Na6	Yes
P580	Na5	Yes
K582	Na5	Yes

*"Contact" is defined by any distance less than 4 Å in the unrefined CPV full structure.
†Nucleic acid number.

metric units of the virus, there was a total of 660 bases observed, accounting for approximately 13% of the encapsidated DNA. Partially ordered nucleic acid structure has also been observed in the spherical viruses bean pod mottle virus,[49] Flockhouse virus,[50] and ϕX174.[25] However, in most other spherical viruses there is no well ordered nucleic acid structure. Conformational differences between the FPV empty and CPV full particle structures occur in the vicinity of the DNA binding site (Fig. 13, Table IX). Many of these residues have expanded into the vacated DNA region of the FPV empty particles (Fig. 13). Similar conformational differences have also been observed between CPV full and CPV empty particles. Thus, the binding of DNA to the internal surface of the parvovirus protein shell inflicts specific conformational changes on the protein. This binding may be associated with recognition by the capsid protein of the parvovirus DNA, although in view of the lack of repeating base sequence the binding cannot be specific for any given sequence. Binding that does not affect base sequence is more likely to be associated with the sugar phosphate backbone. Table IX contains a list of the amino acids in contact with the DNA. The majority of the contacts between the amino acid residues and

nucleic acid are nonspecific hydrophobic interactions. Residues lining this area are 2 alanines, 2 asparagines, 2 glycines, 1 histidine, 1 leucine, 2 lysines, 5 phenylalanines, 2 prolines, 1 serine, 2 threonines, and 1 tyrosine, showing the primarily hydrophobic nature of the pocket.

ACKNOWLEDGMENTS

We thank many helpers in data collection trips (Jodi Bibler, Michael Chapman, Hok-Kin Choi, Vince Giranda, Walter Keller, Prasanna Kolatkar, Iwona Minor, Marcos Oliveira, Andrew Prongay, Liang Tong, Peter Willingmann, and Di Xia) and the outstanding support of the staff at CHESS. We also thank Helene Prongay and Sharon Wilder for help in the preparation of the manuscript; Dan Marinescu and Robert Lynch for introducing us to the parallel processor; and Jodi Bibler, Sanjeev Munshi and Liang Tong for help with the averaging on the Intel 1860 Hypercube. Figures 8, 11, 12, and 13 were generated using the program MacInPlot;[51] Figures 1 and 9 using the program MOLSCRIPT;[52] and Figures 10 and 14 using the program Roadmap.[53] The work was supported by a National Science Foundation research grant and a Lucille P. Markey Charitable Trust grant for the development of structural studies at Purdue to M.G.R.

REFERENCES

1. Siegl, G., Bates, R.C., Berns, K.I., Carter, B.J., Kelly, D.C., Kurstak, E., Tattersall, P. Characteristics and taxonomy of parvoviridae. Intervirology 23:61–73, 1985.
2. Parrish, C.R. Emergence, natural history, and variation of canine, mink, and feline parvoviruses. Adv. Virus Res. 38: 403–450, 1990.
3. Jongeneel, C.V., Sahli, R., McMaster, G.K., Hirt, B. A precise map of splice junctions in the mRNAs of minute virus of mice, an autonomous parvovirus. J. Virol. 59:564–573, 1986.
4. Tratschin, J.-D., McMaster, G.K., Kronauer, G., Siegl, G. Canine parvovirus: relationship to wild-type and vaccine strains of feline panleukopenia virus and mink enteritis virus. J. Gen. Virol. 61:33–41, 1982.
5. Parrish, C.R., Carmichael, L.E., Antczak, D.F. Antigenic relationships between canine parvovirus type 2, feline panleukopenia virus and mink enteritis virus using conventional antisera and monoclonal antibodies. Arch. Virol. 72:267–278, 1982.
6. Parrish, C.R., Aquadro, C.F., Carmichael, L.E. Canine host range and a specific epitope map along with variant sequences in the capsid protein gene of canine parvovirus and related feline, mink, and raccoon parvoviruses. Virology 166:293–307, 1988.
7. Siegl, G. Canine parvovirus: origin and significance of a "new" pathogen. In: "The Parvoviruses." Berns, K.I., ed. New York: Plenum Press, 1984: 363–368.
8. Chapman, M.S., Rossmann, M.G. Structure, sequence and function correlation among parvoviruses. Virology, in press, 1993.
9. Rhode, S.L., III. Nucleotide sequence of the coat protein gene of canine parvovirus. J. Virol. 54:630–633, 1985.
10. Carlson, J., Rushlow, K., Maxwell, I., Maxwell, F., Winston, S., Hahn, W. Cloning and sequence of DNA encoding structural proteins of the autonomous parvovirus feline panleukopenia virus. J. Virol. 55:574–582, 1985.
11. Reed, A.P., Jones, E.V., Miller, T.J. Nucleotide sequence and genome organization of canine parvovirus. J. Virol. 62:266–276, 1988.
12. Parrish, C.R. Mapping specific functions in the capsid structure of canine parvovirus and feline panleukopenia virus using infectious plasmid clones. Virology 183:195–205, 1991.
13. Chang, S.F., Sgro, J.-Y., Parrish, C.R. Multiple amino acids in the capsid structure of canine parvovirus coordinately determine the host range and specific antigenic and hemagglutination properties. J. Virol. 66:6858–6867, 1992.
14. Tsao, J., Chapman, M.S., Agbandje, M., Keller, W., Smith, K., Wu, H., Luo, M., Smith, T.J., Rossmann, M.G., Compans, R.W., Parrish, C.R. The three-dimensional structure of canine parvovirus and its functional implications. Science 251:1456–1464, 1991.
15. Tsao, J., Chapman, M.S., Wu, H., Agbandje, M., Keller, W., Rossmann, M.G. Structure determination of monoclinic canine parvovirus. Acta Crystallogr. B48:75–88, 1992.
16. Wu, H., Keller, W., Rossmann, M.G. Determination and refinement of the canine parvovirus empty capsid structure (submitted).
17. Rossmann, M.G., Arnold, E., Erickson, J.W., Frankenberger, E.A., Griffith, J.P., Hecht, H.J., Johnson, J.E., Kamer, G., Luo, M., Mosser, A.G., Rueckert, R.R., Sherry, B., Vriend, G. Structure of a human common cold virus and functional relationship to other picornaviruses. Nature (London) 317:145–153, 1985.
18. Rossmann, M.G. Conformational adaptations by picornaviruses to antiviral agents and pH changes. In: "Molecular Aspects of Picornavirus Infection and Detection." Semler, B.L., Ehrenfeld, E., eds. Washington, DC: American Society for Microbiology, 1989: 139–154.
19. Rossmann, M.G. The molecular replacement method. Acta Crystallogr. A46:73–82, 1990.
20. Hogle, J.M., Chow, M., Filman, D.J. Three-dimensional structure of poliovirus at 2.9 Å resolution. Science 229: 1358–1365, 1985.
21. Hosur, M.V., Schmidt, T., Tucker, R.C., Johnson, J.E., Gallagher, T.M., Selling, B.H., Rueckert, R.R. Structure of an insect virus at 3.0 Å resolution. Proteins 2:167–176, 1987.
22. Luo, M., Vriend, G., Kamer, G., Minor, I., Arnold, E., Rossmann, M.G., Boege, U., Scraba, D.G., Duke, G.M., Palmenberg, A.C. The atomic structure of Mengo virus at 3.0 Å resolution. Science 235:182–191, 1987.
23. Kim, S., Smith, T.J., Chapman, M.S., Rossmann, M.G., Pevear, D.C., Dutko, F.J., Felock, P.J., Diana, G.D., McKinlay, M.A. Crystal structure of human rhinovirus serotype 1A (HRV1A). J. Mol. Biol. 210:91–111, 1989.
24. Acharya, R., Fry, E., Stuart, D., Fox, G., Rowlands, D., Brown, F. The three-dimensional structure of foot-and-mouth disease virus at 2.9 Å resolution. Nature (London) 337:709–716, 1989.
25. McKenna, R., Xia, D., Willingmann, P., Ilag, L.L., Krishnaswamy, S., Rossmann, M.G., Olson, N.H., Baker, T.S., Incardona, N.L. Atomic structure of single-stranded DNA bacteriophage ϕX174 and its functional implications. Nature (London) 355:137–143, 1992.
26. Crandell, R.A., Fabricant, C.G., Nelson-Rees, W.A. Development, characterization and viral susceptibility of a feline (*Felis catus*) renal cell line (CRFK). In Vitro 9:176–185, 1973.
27. McPherson, A. "Preparation and Analysis of Protein Crystals." New York: Wiley, 1982.
28. Kim, S. Auto-indexing oscillation photographs. J. Appl. Crystallogr. 22:53–60, 1989.
29. Rossmann, M.G. Processing oscillation diffraction data for very large unit cells with an automatic convolution technique and profile fitting. J. Appl. Crystallogr. 12:225–238, 1979.
30. Rossmann, M.G., Leslie, A.G.W., Abdel-Meguid, S.S., Tsukihara, T. Processing and post-refinement of oscillation camera data. J. Appl. Crystallogr. 12:570–581, 1979.
31. Matthews, B.W. Solvent content of protein crystals. J. Mol. Biol. 33:491–497, 1968.
32. Rossmann, M.G., McKenna, R., Tong, L., Xia, D., Dai, J.-B., Wu, H., Choi, H.-K., Lynch, R.E. Molecular replacement real-space averaging. J. Appl. Crystallogr. 25:166–180, 1992.
33. Rossmann, M.G., Blow, D.M. The detection of sub-units within the crystallographic asymmetric unit. Acta Crystallogr. 15:24–31, 1962.
34. Tollin, P., Rossmann, M.G. A description of various rotation function programs. Acta Crystallogr. 21:872–876, 1966.

35. Rao, S.T., Rossmann, M.G. Comparison of super-secondary structures in proteins. J. Mol. Biol. 76:241–256, 1973.
36. Tong, L., Rossmann, M.G. The locked rotation function. Acta Crystallogr. A46:783–792, 1990.
37. Rossmann, M.G. "The Molecular Replacement Method." New York: Gordon & Breach, 1972.
38. McKenna, R., Xia, D., Willingmann, P., Ilag, L.L., Rossmann, M.G. Structure determination of the bacteriophage ϕX174. Acta Crystallogr. B48:499–511, 1992.
39. Jones, T.A. A graphics model building and refinement system for macromolecules. J. Appl. Crystallogr. 11:268–272, 1978.
40. Jones, T.A., Thirup, S. Using known substructures in protein model building and crystallography. EMBO J. 5:819–822, 1986.
41. Truyen, U., Parrish, C.R. Canine and feline host ranges of canine parvovirus and feline panleukopenia virus: Distinct host cell tropisms of each virus *in vitro* and *in vivo*. J. Virol. 66:5399–5408, 1992.
42. Horiuchi, M., Ishiguro, N., Goto, H., Shinagawa, M. Characterization of the stage(s) in the virus replication cycle at which the host-cell specificity of the feline parvovirus subgroup is regulated in canine cells. Virology 189:600–608, 1992.
43. Spalholz, B.A., Tattersall, P. Interaction of minute virus of mice with differentiated cells: Strain-dependent target cell specificity is mediated by intracellular factors. J. Virol. 46:937–943, 1983.
44. Ball-Goodrich, L.J., Tattersall, P. Two amino acid substitutions within the capsid are coordinately required for acquisition of fibrotropism by the lymphotropic strain of minute virus of mice. J. Virol. 66:3415–3423, 1992.
45. Parrish, C.R., Carmichael, L.E., Antczak, D.F. Antigenic relationships between canine parvovirus type 2, feline panleukopenia and mink enteritis virus using conventional antisera and monoclonal antibodies. Arch. Virol. 72: 267–278, 1982.
46. Strassheim, M.L., Gruenberg, A., Veijaleinen, P., Sgro, J.-Y., Parrish, C.R. Two dominant neutralizing antigenic determinants of canine parvovirus are found on the threefold spike of the virus capsid (submitted).
47. Langeveld, J.P.M., Casal, J.I., Vela, C., Dalsgaard, K., Smale, S.H., Puijk, W.C., Meleon, R.H. B-cell epitpoes of canine parvovirus: Distribution on the primary structure and exposure on the viral surface. J. Virol. 67:765–772, 1993.
48. Barbis, D.P., Chang, S.-F., Parrish, C.R. Mutations adjacent to the dimple of the canine parvovirus capsid structure affect sialic acid binding. Virology 191:301–308, 1992.
49. Chen, Z., Stauffacher, C., Schmidt, T., Fisher, A., Johnson, J.E. RNA packaging in bean pod mottle virus. In: "New Aspects of Positive-Strand RNA Viruses." Brinton, M.A., Heinz, F.X., eds. Washington, DC: American Society for Microbiology, 1990: 218–226.
50. Fisher, A.J., Johnson, J.E. Ordered duplex RNA controls capsid architecture in an icosahedral animal virus. Nature (London) 361:176–179, 1993.
51. Smith, T.J. MacInPlot-a program to display electron density and atomic models on the Macintosh personal computer. J. Appl. Crystallogr. 23:141–142, 1990.
52. Kraulis, P. MOLSCRIPT: a program to produce both detailed and schematic plots of protein structures. J. Appl. Crystallogr. 24:946–950, 1991.
53. Chapman, M.S. Mapping the surface properties of macromolecules. Prot. Sci. 2:459–469, 1993.